PRDM14-CtBP1/2-PRC2 complex regulates transcriptional repression during transition from primed to naïve pluripotency

Maiko Yamamoto[1,4], Yoshiaki Suwa[1,4], Kohta Sugiyama[1,4], Naoki Okashita[1,5], Masanori Kawaguchi[1], Naoki Tani[2], Kazumi Matsubara[1], Akira Nakamura[3], and Yoshiyuki Seki[1*]

[1]Department of Biomedical Chemistry, School of Science and Technology, Kwansei Gakuin University, Hyogo, Japan

[2]Liaison Laboratory Research Promotion Center, Institute of Molecular Embryology and Genetics, Kumamoto University, Kumamoto, Japan

[3]Department of Germline Development, Institute of Molecular Embryology and Genetics, Kumamoto University, Kumamoto, Japan

[4]Co-first authors

[5]Present address: Laboratory of Epigenome Dynamics, Graduate School of Frontier Biosciences, Osaka University, 1-3 Yamadaoka, Suita, Osaka 565-0871, Japan

[*]Correspondence: yseki@kwansei.ac.jp

Key words: PRDM14-CtBP1/2-PRC2 complex; transcriptional repression; pluripotency; Embryonic stem cells

JCS Advance Online Article. Posted on 13 July 2020

Summary statement

CRISPR/Cas9-mediated knock out study revealed the molecular hierarchy of PRDM14, CBFA2T2, CtBP1/2 and PRC2 complex, which is required for the transcriptional repression in embryonic stem cells

Abstract

The pluripotency-associated transcriptional network is regulated by a core circuitry of transcription factors. The PR domain-containing protein, PRDM14, maintains pluripotency by activating and repressing transcription in a target gene-dependent manner. However, the mechanisms underlying dichotomic switching of PRDM14-mediated transcriptional control remain elusive. Here, we identified C-terminal binding protein 1/2 (CtBP1/2) as a component of the PRDM14-mediated repressive complex. CtBP1/2 binding to PRDM14 depends on CBFA2T2, a core component of the PRDM14 complex. The loss of *Ctbp1/2* impaired the PRDM14-mediated transcriptional repression required for pluripotency maintenance and transition from primed to naïve pluripotency. Furthermore, CtBP1/2 interacted with the PRC2 complexes, and the loss of *Ctbp1/2* impaired PRC2 and H3K27me3 enrichment at target genes after *Prdm14* induction. These results provide evidence that the target gene-dependent

transcriptional activity of PRDM14 is regulated by partner switching to ensure the transition from primed to naïve pluripotency.

Introduction

Pluripotent cells are common sources of germline- and somatic cells. They are established early in the mammalian embryo. Cellular pluripotency is governed by core transcriptional regulatory circuitry centered on POU5F1 (OCT4) and NANOG (Niwa, 2014). During embryogenesis, *Pou5f1* expression in inner cell mass (ICM) of the blastocyst is maintained in the epiblast and primordial germ cells (PGCs). In contrast, naïve pluripotent markers such as *Nanog*, *Prdm14*, and *Klf2* are repressed during the transition from ICM to epiblast cells. PRDM14 is a sequence-specific transcriptional regulator. Somatic cells maintain *Prdm14* repression. Primordial germ cells (PGCs) specified from most proximal epiblast cells are associated with the reactivation of *Prdm14* expression. This process is necessary for PGC formation (Yamaji et al., 2008) (Nakaki et al., 2013). PGCs are specified by the activation of pluripotency-associated genes, the repression of epiblast markers, and epigenetic reprogramming regulated by repressing major enzymes that methylate DNA and H3K9 (Kurimoto et al., 2008) (Seki et al., 2007) (Ohno et al., 2013) (Kagiwada et al., 2013). We previously showed that PRDM14 induction in epiblast-like cells activates pluripotency-associated genes (*Klf2*, *Tcl1*, *Tfcp2l1*) and represses epiblast markers (*Otx2*, *Dnmt3b* and *Fgf5*). Thus, PRDM14 can both activate and repress transcription depending on the target genes (Okashita et al., 2016). The activation of pluripotent-associated

genes by PRDM14 depends on OCT4 recruitment through TET-mediated DNA demethylation. However, the mechanism by which PRDM14 represses epiblast markers remains unknown (Seki, 2018).

A knockout study showed that PRDM14 shuts off autocrine fibroblast growth factor (FGF) signaling (a crucial differentiation trigger) to maintain mESC pluripotency through the transcriptional repression of *Fgfr1/2* under serum plus LIF (Yamaji et al., 2013). In the presence of the MEK and GSK-3 inhibitors "2i", in addition to LIF, the self-renewal of *Prdm14*-deficient ESCs is maintained because of the repression of FGF signaling via MEKi. SUZ12, one of the Polycomb repressive complex 2 (PRC2) components, is biotinylated by PRDM14 and biotin ligase, which indicates that PRC2 is localized near PRDM14 in the nucleus of ESCs. The loss of *Prdm14* reduces PRC2 and H3K27me3 enrichment at target genes such as *Dnmt3b* and *Fgfr1/2*. Previous studies have not described the biochemical purification of the components of the PRC2 complex with PRDM14 using immunoprecipitation analysis from ESC nuclear lysates (Nady et al., 2015; Tu et al., 2016). Instead, a co-repressor protein CBFA2T2 was identified as a core component of the PRDM14 complex. CBFA2T2 directly interacts with PRDM14 to form a scaffold that stabilizes PRDM14 on the chromatin and regulates target gene

transcription and repression. The *Cbfa2t2* KO phenotypes are nearly identical to those of *Prdm14* KO in ESC and PGC development. These findings demonstrated that CBFA2T2 is an essential component of the PRDM14 complex for both transcriptional activation and repression. However, how dichotomic switching of the target gene-dependent transcriptional activity of PRDM14 is operated remains unknown.

Here, we investigated the *N*-terminal domain of PRDM14, which has no discernable functional domain, and its contribution to the maintenance of pluripotency. We performed a mass spectrometry analysis of PRDM14-containing complex to disclose partner molecules that bind to the *N*-terminal domain of PRDM14. Knockout models of *Ctbp1/2*, *Suz12,* and *Cbfa2t2* were employed to delineate possible interactions between CTBP1/2 and PRDM14-CBFA2T2 complex with PRC2 at repressed target genes in ESCs.

Results

Functional domain mapping of PRDM14 in pluripotency induction and maintenance

Several studies demonstrated that PRDM14 controls the transcriptional networks required for pluripotency. These include the self-renewal of embryonic stem cells (ESCs) cultured in serum plus LIF (Yamaji et al., 2013), LIF-independent self-renewal of ESCs (Okashita et al., 2015), and conversion from epiblast-like cells (EpiLCs) to ESCs (Okashita et al., 2016) (Supplemental Fig. S1A). To elucidate the functional domain of PRDM14 regulating mESC pluripotency, we established a doxycycline-inducible expression systems of full-length PRDM14 and PRDM14 mutants lacking *N*-terminal- or PR domain in *Prdm14*-deficient mESCs (Fig. 1A, Supplemental Fig. S1B). In the absence of doxycycline and hence *Prdm14* expression, cell lines could not expand beyond four passages over 8 d in serum plus LIF (Supplemental Fig. S1C, D). This observation was consistent with a previous report (Yamaji et al., 2013). *Prdm14*-deficient mESCs expressing exogenous full-length PRDM14 could expand and retain alkaline phosphatase activity in serum plus LIF condition. Deletion of the *N*-terminal domain of PRDM14 completely eliminated the maintenance of mESC pluripotency whereas PRDM14 without PR domain expression partially supported the self-renewal activity of *Prdm14*-deficient mESCs in serum plus LIF. To analyze the functional domain of PRDM14 in LIF-independent

self-renewal of ESCs (Okashita et al., 2015), we created ESCs in which full-length PRDM14 and PRDM14 mutants lacking *N*-terminal- or PR domain are induced by doxycycline administration (Fig. 1A,B). Overexpression of full-length PRDM14 in ESCs maintained alkaline phosphatase (AP) activity in the absence of LIF, while the maintenance of pluripotency was diminished by the deletion of N-terminal or PR domain (Supplementary Fig. S1E). ESCs can be differentiated into epiblast-like cells (EpiLCs) by the stimulation of Activin A, bFGF, and 1% knockout serum replacement (KSR) associated with the down-regulation of pluripotency-associated factors and the upregulation of epiblast markers(Hayashi et al., 2011). Consistent with our previous study (Okashita et al., 2016), EpiLCs with the overexpression of full-length PRDM14 retained the AP activity in the S/L condition similar to ESCs (Fig. 1C, D). However, the deletion of the N-terminal region or PR domain of PRDM14 significantly impaired the conversion efficiency from EpiLCs into ESCs. Thus, although the *N*-terminal region of PRDM14 does not have a discernable functional domain apparent in its primary sequence, it is essential for pluripotency induction and maintenance.

Identification of the components of PRDM14 complex in ESCs

We sought for components of PRDM14 complex by shotgun liquid chromatography-tandem mass spectrometry (LC-MS/MS). PRDM14 complex was immunopurified with anti-FLAG antibody from whole cell lysates of ESCs expressing FLAG-PRDM14, FLAG-PRDM14ΔN, and FLAG-PRDM14ΔPR cultured in serum plus LIF, and separated by SDS-PAGE. MS analysis of silver-stained proteins of immunoprecipitants showed that the deletion of the *N*-terminal region of PRDM14 significantly reduced the proteins co-immunoprecipitated with PRDM14 (Fig. 1E). Consistent with a previous study (Nady et al., 2015; Tu et al., 2016), CBFA2T2 was found to be a major component of the PRDM14 complex (Fig. 1F). CBFA2T2 was detected in the full length PRDM14 complex, but absent in ΔN and ΔPR PRDM14 complexes, indicating that interaction between PRDM14 and CBFA2T2 depended on both the *N*-terminal region and the PR domain. MS analysis also identified proteins that are known components of the NODE, esBAF and CRL4 complexes, and CtBP2 (Liang et al., 2008) (Ho et al., 2009a) (Gao et al., 2015). Western blot analysis of PRDM14 immuno-precipitates confirmed the interaction of PRDM14 with the aforementioned molecules (Fig. 1G). Proximity-dependent biotin identification (BioID) methods detected the interaction of

PRDM14 with the components of the polycomb repressive complex 2 (PRC2) in ESCs (Yamaji et al., 2013). However, our immunoprecipitation assay using antibody against FLAG-PRDM14 followed by MS analysis did not detect the components of PRC2. Other researchers also failed to detect the components of PRC2 by immunoprecipitation of PRDM14 complex followed by MS (Nady et al., 2015) (Tu et al., 2016). This suggested that the interaction between PRDM14 and PRC2 components may be very weak, transient, and/or indirect, such that the interaction could not be detected by the IP-MS strategy we used.

In this study, we focused on *C*-terminal binding protein 2 (CtBP2) in the components of the PRDM14 complex because CtBP2 is reported to recruit the PRC2 complex at the target genes (Kim et al., 2015). Immunoprecipitation of CtBP2 followed by western blot with anti-FLAG antibody confirmed the interaction between CtBP2 and PRDM14 (Fig. 1H). LC-MS/MS of the PRDM14 complex indicated that, similar to the case for CBFA2T2, CtBP2 was present only in the full-length PRDM14 complex (Fig. 1F). Intriguingly, there were fewer peptides detected that matched CtBP2 compared with those matching CBFA2T2. Given that the latter is a direct stoichiometric partner of PRDM14 (Nady et al., 2015), PRDM14 might indirectly interact with CtBP2 via CBFA2T2 in the ESCs. We therefore created *Cbfa2t2* KO ESCs

carrying a doxycycline-inducible *Prdm14* expression unit to determine whether the interaction between PRDM14 and CtBP2 is CBFA2T2 dependent (Supplemental Fig. S2A). As in the case of *Prdm14* KO ESCs, because *Cbfa2t2* KO ESCs could not be maintained in serum plus LIF condition (Tu et al., 2016), we screened for the interaction between PRDM14 and CtBP2 in ESCs lacking *Cbfat2t2* under 2i plus LIF condition. PRDM14 also interacted with CtBP2 in ground state wild type ESCs, although the interaction of PRDM14 with CtBP2 was significantly impaired in the absence of *Cbfa2t2* (Fig. 1I). These results indicate that the PRDM14-CtBP2 interaction is CBFA2T2-dependent, suggesting that PRDM14 indirectly interacts with CtBP2 through CBFA2T2 in ESCs.

PRDM14 recruits CtBP2 at the repressive targets

To investigate whether PRDM14- and CtBP2-binding on the genome overlapped in mESCs, we reconstructed ChIP-seq tag mapping for PRDM14 and CtBP2 near the PRDM14 binding regions using published datasets (Kim et al., 2015; Ma et al., 2011). We found that over 50% of CtBP2-binding peaks were enriched and overlapped with the PRDM14-binding peaks in mESCs (Fig. 2A,B). To examine if CtBP2 recruitment at the PRDM14's target genes (*Dnmt3b*, *Zfp281*, and *Id1*) (Fig. 2C) depended on PRDM14, we used ChIP-qPCR to compare the

PRDM14 and CtBP2 enrichments at these genes before and after *Prdm14* induction under serum plus LIF condition (Fig. 2D). Two days after *Prdm14* induction, FLAG-PRDM14 was significantly enriched at loci of all the genes, and CtBP2 and HDAC1 enrichments to these loci were also upregulated. In contrast, H3 lysine acetylation (H3KAc) was decreased by *Prdm14* induction at all loci. These results show that the recruitment of the CtBP2-HDAC1 repressive complex at these repressive target genes is PRDM14 dependent.

We previously showed that PRDM14 overexpression reduces promoter cytosine methylation of pluripotency-associated- and germline-specific genes through the recruitment of ten-eleven translocation (TET) proteins, resulting in upregulation of these target genes (Okashita et al., 2014). To investigate the switching of PRDM14 complexes in the target-dependent manners, we compared CtBP2 enrichment before and after *Prdm14* induction at pluripotency-associated- and germline-specific genes. Publicly accessible ChIP-seq data showed that CtBP2 was not colocalized with PRDM14 at *Tcl1*, *Dppa3*, and *Tfap2c* (Fig. 2E). Unlike the repressive target genes, CtBP2 enrichment was significantly decreased by *Prdm14* induction, whereas TET1 enrichment was consistently increased by *Prdm14* induction at *Tcl1*, *Dppa3* and *Tfap2c* (Fig. 2F). Contrary to the interaction of PRDM14 with CtBP2 through CBFA2T2, pull-down assay

using recombinant proteins of FLAG-PRDM14 and HA-TET2 showed that PRDM14 directly interacted with TET2 in the absence of CBFA2T2 (Fig. 2G). Further, we performed a sequential ChIP for PRDM14 followed by CtBP2 or TET1 and showed that PRDM14 and CtBP2 or TET1 co-occupied at target genes (Fig. 2H,I). These findings demonstrate that the recruitment PRDM14 partners on target genes varied between activating and repressing loci, suggesting that differences in the compositions of PRDM14 complexes on each target gene may account for dichotomic transcriptional switch of PRDM14.

PRC2 is required for PRDM14-dependent transcriptional repression

To establish whether CtBP2 mediates PRDM14 recruitment of the PRC2 complex, we compared H3K27me3 distribution near the PRDM14- and CtBP2-binding regions and the PRDM14-CtBP2 co-binding region in ESCs using published ChIP-seq datasets. H3K27me3 distribution near the PRDM14-binding regions was significantly lower than those near the CtBP2-binding regions. However, the H3K27me3 levels near the PRDM14-CtBP2 co-binding regions were substantially higher than those near the CtBP2-binding regions (Fig. 3A). These results suggest that PRDM14 and CtBP2 coordinately regulate H3K27me3 levels at the silenced genes in mESCs, presumably by recruiting the PRC2 complex that methylates H3K27.

To determine whether PRDM14 recruits the PRC2 complex at the target genes, we compared SUZ12, a central component of PRC2 and H3K27me3 enrichment at the target gene levels before and after *Prdm14* induction in mESCs under serum plus LIF condition. Two days after *Prdm14* induction, SUZ12 and H3K27 were consistently elevated at the target genes except for *Id1* (Fig. 3B). Co-immunoprecipitation analysis disclosed a weak interaction between PRDM14 and SUZ12 (Fig. 3C). Consistent with a previous study, we found a more efficient co-immunoprecipitation of SUZ12 with CtBP2 (Fig. 3D). Therefore, PRDM14 appears to recruit the PRC2 complex at target genes mediated by CtBP2.

To elucidate the function of PRC2 in transcriptional regulation by PRDM14, we used a CRISPR/Cas9 system to create *Suz12* knockout ESCs with the doxycycline-dependent *Prdm14* expression. We used a frameshift mutation to design a gRNA at exon 6 of the *Suz12* genomic region and delete the zinc finger domain located at the *C*-terminal region (Supplementary Fig. 2B). Western blot analysis showed complete deletion of the SUZ12 proteins and significant reduction of genome-wide H3K27 methylation in *Suz1*2 KO ESCs (Fig. 3E,F). Comparison of the PRDM14-downregulated genes between the wild type and *Suz12* KO ESCs indicated that

repression of *Dnmt3l*, *Dnmt3b*, and *Gja1* by PRDM14 was significantly impaired in *Suz12* KO ESCs (Fig. 3G). Furthermore, although *Prdm14* has negative feedback activity and represses its own transcription in mESCs (Okashita et al., 2014), *Suz12* KO significantly upregulated endogenous *Prdm14*. Thus, SUZ12 is required for negative *Prdm14* feedback and/or active *Prdm14* repression by unknown factors in mESCs.

To analyze the global impact of *Suz12* KO in transcriptional PRDM14 regulation, we performed a microarray analysis to compare the effects of PRDM14 on relative gene expression in wild type and *Suz12* KO ESCs. The PRDM14-mediated gene upregulation and downregulation observed in the wild type ESCs were globally impaired in the *Suz12* KO (Fig. 3H). To confirm the results of microarray analysis, we performed qRT-PCR on selected genes (Fig. 3I,J). In *Suz12* KO ESCs, PRDM14-mediated upregulation of the early PGC markers was moderately impaired, whereas downregulation of the epiblast markers by PRDM14 was consistently disordered.

CtBP1/2 is partially required for PRDM14-mediated transcriptional repression

We used the CRISPR/Cas9 system to create *Ctbp2* single knockout and *Ctbp1/2* double knockout (DKO) ESCs with doxycycline-dependent *Prdm14* expression. We deleted the *Ctbp1* start codon and inserted the stop codon in *CtBP2* (Supplementary Fig. 2C). Consequently, these proteins were completely eliminated (Fig. 4A). *Ctbp2* deletion flattened the formerly dome-like mESC colonies (Fig. 4B). Immunofluorescence and western blotting analysis showed that the protein levels of OCT4 were maintained in *Ctbp1/2* DKO ESCs as observed in wild type ESCs (Fig. 4C,D). Wild type ESCs showed the heterogeneous expression of NANOG, while its was homogeneous in *Ctbp1/2* DKO ESCs (Fig. 4C). Furthermore, the protein levels of NANOG was significantly elevated in *Ctbp1/2* DKO ESCs, suggesting that the loss of *Ctbp1/2* stabilizes the pluripotent network of transcription factors in ESCs under serum plus LIF condition (Fig. 4D). Next, we used microarray analysis to assess the impact of *Ctbp1/2* loss on PRDM14-mediated transcriptional regulation in ESCs by comparing expression levels between the wild type and *Ctbp1/2* DKO ESCs. Unlike the *Suz12* KO phenotype, PRDM14-mediated transcriptional activation in *Ctbp1/2* DKO ESCs was relatively stable, whereas PRDM14-mediated transcriptional repression was significantly impaired (Fig. 4E,F). The results of the

microarray analysis were corroborated by qRT-PCR (Fig. 4G). Unexpectedly, some early PGC markers (*Dppa3* and *Rhox6*) were significantly repressed in *Ctbp1/2* DKO ESCs. To determine whether CtBP2 participates in PRDM14-mediated repression of *Dnmt3b* transcription, we evaluated the effect of *Ctbp1/2* loss on *Dnmt3b* promoter activity regulated by PRDM14. *Dnmt3b* promoter activity was suppressed by PRDM14 expression in wild type but not *Ctbp1/2* DKO ESCs (Fig. 4H). To clarify the hierarchy of PRDM14, CtBP2, and SUZ12 in PRDM14-mediated repression of *Dnmt3b* transcription, we compared PRDM14, SUZ12, and H3K27me3 enrichment on the *Dnmt3b* loci of wild type and *CtBP1/*2 DKO ESCs before and after *Prdm14* induction. PRDM14 recruitment was significantly impaired by *Ctbp*1/2 loss. In wild type ESCs, SUZ12 and H3K27me3 enrichments were significantly elevated on the *Dnmt3b* loci after *Prdm14* induction, whereas they were completely abolished by *CtBP1/2* loss (Fig. 4I). Therefore, there is an absolute requirement for CtBP1/2 in the repression of *Dnmt3b* transcription by PRDM14 in ESCs.

Suz12 is required for PRDM14-induced reversion from EpiLCs to ESCs

We have previously shown that PRDM14 overexpression converts EpiLCs to ESCs (Okashita et al., 2016). We therefore examined the role of the CtBP1/2/PRC2 axis in EpiLCs to ESCs

conversion in response to PRDM14 overexpression. Before this process, ESCs must be cultured in 2i plus LIF medium to promote ground-state pluripotency (Hayashi et al., 2011). Unexpectedly, cell transfer from S/L to 2i/L caused an abnormality in the *Ctbp1/2* KO ESCs growth rate as shown in Fig. 7A. Thus, we could not investigate the function of CtBP2 in the EpiLC experiments. To clarify the function of SUZ12 in PRDM14-associated pluripotency, we compared the conversion efficiency between wild type and *Suz12* KO EpiLCs based on the number of AP-positive colonies and found that PRDM14-induced transformation from EpiLCs to ESCs was significantly impaired in the *Suz12* KO background (Fig. 5A-D). RT-qPCR analysis showed that the activation of pluripotency-associated genes and the repression of differentiation markers were both diminished in *Suz12* KO (Fig. 5E,F). Thus, PRDM14 cooperates with SUZ12 to convert EpiLCs to ESCs by activating pluripotency-associated genes and repressing differentiation markers.

SUZ12-CtBP1/2 is required for transcriptional Dnmt3b/l repression in the ground state

Transfer of ESCs from serum plus LIF (S/L) to 2i plus LIF (2i/L) upregulates *Prdm14* which, in turn, downregulates *Dnmt3a/b/l* (Habibi et al., 2013). We determined whether *Suz12* and *Ctbp1/2* are required for the repression of *Dnmt3a/b/l* transcription during the transition from

metastable- to ground-state pluripotency. Transfer of both wild type and *Suz12* KO ESCs from S/L to 2i/L produced the dome-shaped colonies characteristic of ground-state pluripotency associated with the elevation of *Prdm14* expression (Figu. 6A). Alkaline phosphatase activity was heterogeneous in wild type and *Suz12* ESCs uder S/L condition, while gound state ESCs derived from wild type and *Suz12* KO ESCs showed homogeneous staining of alkaline phosphatase activity (Fig. 6B). Contrary to the upregulation of *Prdm14*, *Dnmt3b/l* repression was significantly diminished in *Suz12* KO ESCs in 2i/L condition (Fig. 6C). In contrast, the DNMT3B protein level was significantly reduced in *Suz12* KO ESCs cultured in 2i/L (Fig. 6D). We compared the DNMT3B protein levels in 2i/L and S/L following PRDM14 induction. DNMT3B was relatively constant after *Prdm14* induction in S/L (Fig. 6E).

Next, we compared *Dnmt3a/b/l* expression between wild type and *Ctbp1/2* DKO ESCs. The *Ctbp1/2* DKO ESC colonies were smaller than those of wild type ESCs after three passages in 2i/L (Fig. 6F) and AP activity of the *Ctbp1/2* DKO ESC colonies was very weak compared with wild type ESCs under 2i plus LIF condition (Fig. 6G). We isolated mRNA and proteins from *Ctbp1/2* DKO ESCs cultured in 2i/L for three passages and compared *Dnmt3a/b/l* expression. *Dnmt3b/l* repression induced by 2i/L condition was diminished in *Ctbp1/2* DKO ESCs (Fig. 6H). Therefore, CtBP1/2 is essential for transcriptional *Dnmt3b/l* repression in ground-state

ESCs. As observed in *Suz12* KO ESCs, the DNMT3B protein levels were reduced in *Ctbp1/2* DKO ESCs in 2i/L but not in *Ctbp1/2* DKO ESCs following PRDM14 induction in serum plus LIF (Fig. 6I,J).

Ctbp1/2 is required to maintain ground-state pluripotency

To determine the onset of *Ctbp1/2* KO ESC abnormality during the transition from S/L to 2i/L, we compared the morphology of *Ctbp1/2* KO ESCs with that of wild type ESCs every 2 days. Wild type ESCs presented with both dome-shaped and flat colonies in S/L (Fig. 7A). Six days after the transfer from S/L to 2i/L, the wild type ESCs produced the dome-shaped colonies characteristic of ground-state pluripotency. In contrast, six days after transfer from serum plus LIF to 2i plus LIF, the *Ctbp1/2* DKO ESCs failed to form the clear dome-shaped morphology indicative of ground-state pluripotency. The growth of *Ctbp1/2* DKO ESCs was slower than that of wild ESCs at 4–6 d after transfer from S/L to 2i/L (Fig. 7B). Apoptosis had slightly increased and the proportion of cells in S-phase was significantly reduced in *Ctbp1/2* DKO ESCs relative to wild type ESCs at 4 d after transfer to 2i/L (Fig. 7C, D).

Discussion

Prdm14 regulates pluripotent and primordial germ cells in mice via target gene-dependent transcriptional activation and repression (Okashita et al., 2016) (Nakaki et al., 2013) (Yamaji et al., 2013). To understand the transcriptional activity switching mechanism in the PRDM14 complex, we performed a proteomics analysis of the PRDM14 complex in ESCs. We identified CtBP1/2 as a critical component of PRDM14-mediated transcriptional repression. The repressive marker of histone modification H3K27me3 was enriched near the PRDM14 and CtBP2 co-occupied regions in mESCs. CtBP1/2 was required to increase SUZ12 and H3K27me3 binding at the repressive PRDM14 targets. Thus, PRDM14 establishes the transcriptional networks for pluripotency mediated by recruiting the CtBP1/2-PRC2 complex.

In mice, *Prdm14* is activated in most proximal epiblast cells to induce primordial germ cells (PGCs) (Yamaji et al., 2008) (Nakaki et al., 2013). Our previous study showed that PRDM14 regulates transcriptional activation and repression in a target gene-dependent manner (Okashita et al., 2016). Our MS analysis identified the molecules involved in transcriptional activation including the esBAF complex (Ho et al., 2009b) and those participating in transcriptional repression including the NODE complex (Liang et al., 2008). These components of the

PRDM14 complex are evidence that PRDM14 switches its transcriptional activity by forming various complexes depending on the target genes involved. CBFA2T2 is a core partner of PRDM14 and essential for PRDM14-mediated transcriptional activation and repression (Nady et al., 2015) (Tu et al., 2016). PRDM14 co-evolved with CBFA2T during deuterostome evolution, which strongly suggests the functional dependence of PRDM14 on CBFA2T2 (Kawaguchi et al., 2019). The nervy homology 2 domain (NHR2) of CBFA2T2 participates in homotypic and heterotypic oligomerization which may serve as an interaction surface for the partner molecules of PRDM14. Our data showed that the loss of *Cbfa2t2* diminished the interaction between PRDM14 and CtBP2 in mESCs, which clearly supports the idea that CBFA2T2 oligomer acts as an interaction surface of PRDM14 complex.

Conflicting results for the interaction between PRDM14 and PRC2 have been reported (Tu et al., 2016) (Nady et al., 2015) (Yamaji et al., 2013). Here, soon after PRDM14 expression was induced, the SUZ12 and H3K27me3 levels were significantly increased at the repressive PRDM14 target genes. We also showed that SUZ12 interacts with both PRDM14 and CtBP2 in mESC. Our knockout studies clearly provide evidence that PRDM14 recruits the PRC2 complex through CBFA2T2 and CtBP1/2 at the repressive PRDM14 complex targets. This

discovery may resolve the discrepancy of the previous study concerning the interaction between the PRDM14 and PRC2 complexes.

Global DNA methylation decreases during the transition from metastable- to ground-state pluripotency associated with transcriptional repression of *Dnmt3a*/*b*/*l* by upregulating *Prdm14* (Habibi et al., 2013) (Yamaji et al., 2013). Here, although transcriptional *Dnmt3b/l* repression was significantly diminished, its protein levels were reduced in *Suz12* KO- and *Ctbp1/2* DKO ESCs under 2i/L condition. These findings indicate post-transcriptional DNMT3A/B regulation in ground-state ESCs. Consistent with our results, *Prdm14* upregulation in 2i/L induces ubiquitin-dependent DNMT3A/B degradation (Sim et al., 2017). PRDM14 forms a ternary complex with G9A and DNMT3A/B. G9A-mediated lysine methylation of DNMT3A/B triggers ubiquitin-dependent protein degradation. In this study, DNMT3B protein levels were relatively stable after *Prdm14* induction in *Suz12* and *Ctbp1/2* DKO ESCs under S/L condition. Therefore, ubiquitin-dependent DNMT3A/B protein degradation is controlled by both PRDM14 induction and 2i. Our MS analysis of PRDM14 did not disclose G9A or DNMT3B in S/L. The interactions of PRDM14 with G9A and DNMT3B might be enhanced by 2i, which governs ubiquitin-dependent DNMT3A/B protein degradation in ground-state ESCs.

We discovered that CtBP1/2 maintains ground-state pluripotency. As *Prdm14*-deficient ESCs can be expanded in 2i/L (Yamaji et al., 2013), the function of CtBP1/2 in ground-state pluripotency maintenance is independent of that of PRDM14. The phenotype of *Ctbp1/2* DKO in ground-state ESCs resembles that of *Klf2* KO ESCs cultured in 2i (Yeo et al., 2014). There was an abnormal upregulation of PGC-markers in *Klf2* KO ESCs under 2i condition. In contrast, the expression of PGC-markers in *Ctbp1/2* DKO ESCs were similar to those in wild type ESCs under 2i/L condition (data not shown). These observations imply that the molecular pathways responsible for ESC abnormality under 2i condition can be distinguished between *Klf2* KO and *Ctbp1/2* DKO. The mechanistic insight for the abnormality of ground state pluripotency caused by the loss of *Ctbp1/2* DKO warrants further investigation.

Here, we established that the target-dependent transcriptional activity of PRDM14 is defined by the partner switching in the re-establishment of transcription factor network for naïve pluripotency. Further study will be needed to unravel the mechanism of PRDM14 complex target-dependent gene recognition.

Materials and Methods

Cell culture

E14tg2a ESCs were cultured in Glasgow Minimum Essential Medium (GMEM) (Wako Pure Chemical Industries, Ltd., Osaka, Japan) containing 10% fetal calf serum (FCS; Invitrogen, Carlsbad, CA, USA), 1 mM glutamine (Wako Pure Chemical Industries, Ltd.), nonessential amino acid (Wako Pure Chemical Industries, Ltd.), and 0.1 mM 2-mercaptoethanol (Wako Pure Chemical Industries, Ltd.). The culture was supplemented with leukemia inhibitory factor (LIF; Wako Pure Chemical Industries, Ltd.) in the absence of feeder cells.

Induction of epiblast-like cells (EpiLCs)

ESCs were cultured in N2B27 medium with 3 μM CHIR99021 (Sigma-Aldrich, St Louis, USA), 0.4 μM PD0325901 (Wako Pure Chemical Industries, Ltd.), and LIF on a dish coated with 0.01% (w/v) poly-*L*-ornithine (Millipore EMD, Billerica, MA, USA) and 10 ng mL^{-1} laminin (BD Bioscience). EpiLC induction was performed as previously described, with minor modifications (Hayashi et al., 2011). EpiLCs were induced from ESCs in N2B27 basal medium containing 20 ng mL^{-1} activin A (PeproTech, London, UK) and 0.1% (w/v)

StemSure® Serum replacement (SSR) (Wako Pure Chemical Industries, Ltd.) for 3 d on a dish coated with 16.7 μg mL^{-1} human plasma fibronectin (Millipore EMD). After EpiLC induction, the cells were collected and replated with or without doxycycline in GK15 medium on a dish coated with 16.7 μg mL^{-1} human plasma fibronectin (Millipore EMD). For the colony formation assay of AP-positive cells, ESCs, EpiLCs, and EpiLCs with or without PRDM14 were dissociated by TrypLE Select (Invitrogen). Cells (10^4) were cultured under standard ESC culture conditions. After culturing for 3 d, the cells were stained for alkaline phosphatase activity.

Generation of knockout ESCs using a CRISPR-Cas9 system

Guide RNAs for *Cbfa2t2*, *Suz12*, and *CtBP1/2* were generated in pX330-U6-Chimeric_BB-CBh-hSpCas9, which was gift from Fen Zhang (Addgene plasmid #42230) (Cong et al., 2013). The guide RNA sequences are listed in Supplementary Table 1. The pX330 was co-transfected with pCAG-EGFP into induced PRDM14 ESCs (Okashita et al., 2016). The GFP-positive fraction was sorted by Cell Sorter (No. SH800; Sony Biotechnology, Inc., Tokyo, Japan). Genomic DNA deletions were sequenced and lack of protein expression was confirmed by western blot.

Immunoprecipitation and western blot

Cells were lysed in immunoprecipitation buffer (50 mM Tris-HCl (pH 8.0), 150 mM NaCl, 1% (w/v) NP40, and 0.1% (w/v) Triton X-100). Lysates were incubated with anti-FLAG- or anti-CtBP2 antibody captured with protein G- or protein A magnetic beads (Bio-Rad Laboratories, Hercules, USA). Protein complexes were washed thrice with a buffer composed of 50 mM Tris-HCl (pH 8.0), 5 M NaCl, and 0.1% (w/v) NP40 and eluted with glycine buffer (pH 2.0). Immunoprecipitants were denatured with 2-mercaptoethanol, separated on polyacrylamide-SDS gels, and blotted on polyvinylidene fluoride (PVDF) membranes. Proteins on the membranes were probed using the following primary antibodies: α-FLAG (Sigma-Aldrich; F1804, 1/500) , α-CBFA2T2 (Bethyl Laboratories, Inc.; A303-593A, 1/500), α-CtBP2 (BD Biosciences; 612044, 1/1000), α-BRG1 (Merck Millipore; 07-478, 1/1000), α-DDB1 (Abcam; ab109027, 1/500), α-CUL4B (Proteintech; 12916-1-AP, 1/1000), α-PRMT5 (Merck Millipore; 07-405, 1/1000), and α-MOV10 (Proteintech; 10307-1-AP, 1/1000). The membranes were incubated with horseradish peroxidase-coupled secondary antibodies. All antibodies were detected with Immunostar LD (Wako Pure Chemical Industries, Ltd.)

In vitro protein synthesis and pull-down assay

FLAG-PRDM14 and HA-TET2 proteins were synthesized by Human Cell-Free Protein Expression System (Takara Bio Inc., Shiga, Japan) according to the manufacturer's instruction. FLAG-PRDM14 and HA-TET2 were incubated in a binding buffer (20 mM Tris-HCl (pH 8.0), 100 mM KCl, 5 mM $MgCl_2$, 2 mM DTT, 0.1% Triton X-100, 1 mM Phenylmethanesulfonyl fluoride（PMSF) at 4℃ for 3 hrs. The mixture was incubated with Rat anti-HA antibody (Roche, 3F10) and captured with protein G magnetic beads, followed by western blotting with anti-FLAG antibody.

Protein identification by mass spectrometry

The immunoprecipitated proteins were separated on polyacrylamide-SDS gel and stained with Silver Stain for Mass Spectrometry (Thermo Fisher Scientific, Waltham, MA, USA). For the in-gel digestion of proteins, each lane was excised into 13-14 gel slices and the slices cut into approximately 1-mm pieces. Proteins in the gel pieces were reduced with DTT (Thermo Fisher Scientific), alkylated with iodoacetamide (Thermo Fisher Scientific), and digested with trypsin (Promega, Madison, WI, USA) or Trypsin/Lys-C Mix, Mass Spec Grad (Promega) in a buffer containing 40 mM ammonium bicarbonate (pH 8.0) overnight at 37ºC. The resultant peptides

were analyzed on an Advance UHPLC system (AMR, Tokyo, Japan) coupled to a Q Exactive mass spectrometer (Thermo Fisher Scientific) and the raw mass spectrum processed using Xcalibur (Thermo Fisher Scientific). The raw LC-MS/MS data was analyzed against the SwissProt database or the NCBI nonredundant protein database restricted to *Mus musculus* using Proteome Discoverer version 1.4 (Thermo Fisher Scientific) with the Mascot search engine version 2.4 (Matrix Science, London, UK). A decoy database comprised of either randomized or reversed sequences in the target database was used for false discovery rate (FDR) estimation, and Percolator algorithm was used to evaluate false positives. Search results were filtered against 1% global FDR for high confidence level.

Chromatin immunoprecipitation (ChIP) and sequential ChIP

Cells were cross-linked with 1% (w/v) paraformaldehyde for 10 min at room temperature. Cross-linked cells were lysed with sodium dodecyl sulfate (SDS) buffer. Cross-linked DNA/protein complexes were sheared in a Covaris M220 system (Covaris Instruments). DNA/protein complexes were incubated with anti-FLAG, anti-CtBP2, anti-HDAC1 (Abcam; ab46985), anti-TET1 (Merck Millipore; 09-872), anti-TET2 (Abcam; 124297), and anti-H3KAc (Merck Millipore; 06-599) antibodies at 4°C for 12 h. The antibody/protein/DNA

complexes were corrected by protein A or protein G SureBeads (Bio-Rad Laboratories). De-fixed DNA was purified by phenol/chloroform extraction and precipitated with ethanol. For re-ChIP analysis, the antibody/protein/DNA complexes were recovered by TE (10 mM Tris-HCl (pH8.0), 1 mM EDTA) containing 20 mM DL-Dithiothretiol (DTT) and followed by 2nd immunoprecipitation. Enrichment of the proteins on the genome was analyzed by qPCR using the primers listed in Supplementary Table 1.

Microarray and data analyses

Total RNA was purified with a PureLink^{TM} RNA Mini Kit (Ambion, Inc.). Purified total RNA (150 ng) was labeled with a GeneChip^{TM} WT PLUS reagent kit (Thermo Fisher Scientific,) and hybridized to a GeneChip^{TM} Mouse Gene 2.1 ST array strip (Thermo Fisher Scientific) according to the manufacturer's instructions. The CELL files of the GenChIP data were normalized by robust multi-array average (RMA) at the default setting in Affymetrix Expression Console^{TM} (Thermo Fisher Scientific). Expression data were visualized with R and Cluster 3.0 software. Data has been deposited in the GEO databases under accession number GSE134666.

Immunofluorescence analysis

Cells were treated with PBS containing 0.5% Triton-X to permeabilize. Premeabilized cells were incubated with 1st antibody solution containing anti-OCT4 antibody (Santa Cruz Biotechnology, Inc. Sc-8628; 1/500) or anti-NANOG antibody (eBioscience™, 14-5761-80, 1:500), and followed by Alexa 555 anti-Mouse (abcam, ab150106; 1/500) or DyLight anti-Rat (ROCKLAND, 612-142-120; 1/500) secondary antibody reaction.

Analysis of apoptotic cells and cell cycle distribution

To detect apoptotic cells, wild type and *Ctbp1/2* DKO ESCs cultured in serum LIF or 2i/LIF were stained with fluorescein isothiocyanate (FITC)-conjugated annexin V and propidium iodide (PI) according to the manufacturer's protocol (Nacalai Tesque, Kyoto, Japan). Cell cycle distributions were determined by PI staining followed by flow cytometry (Seki et al., 2007) .

Author contributions

M. Y., Y. Suwa, and K. S. performed most of the experiments and analyzed the data. N. T. performed mass spectrometry. A. N. provided feedback on the immunoprecipitation analysis and contributed to writing the manuscript. Y. Seki designed and performed the experiments and wrote the manuscript. All authors discussed the results and approved the final version of the manuscript.

Acknowledgments

We would like to thank all member of the Seki laboratory for stimulating discussion.

Conflict of interest

The authors declare no competing or financial interests

Funding

This study was supported by a Grant-in-Aid for Young Scientists (A) (Japan Society for the Promotion of Science KAKENHI grant number 24681040), a Grant-in-Aid for Scientific Research (B) (Japan Society for the Promotion of Science KAKENHI grant number

18H02422), the Promotion of Joint International Research (Japan Society for the Promotion of Science KAKENHI grant number 15KK0262), the Scientific Research on Innovative Areas, ‘Epigenome dynamics and regulation in germ cells’ (Ministry of Education, Culture, Sports, Science, and Technology KAKENHI grant numbers 26112514 and 16H01223), the Scientific Research on Innovative Areas, ‘Mechanisms regulating gamete formation in animals’ (Ministry of Education, Culture, Sports, Science, and Technology KAKENHI grant number 16H01258), and the Scientific Research on Innovative Areas, ‘Program of totipotency: From decoding to designing’ (Ministry of Education, Culture, Sports, Science, and Technology KAKENHI grant number 20H05375). This work was supported by the program of the Joint Usage/Research Center for Developmental Medicine, Institute of Molecular Embryology and Genetics, Kumamoto University.

Data availability

Microarray data has been deposited in Gene Expression Omnibus (GSE134666).

References

Cong, L., Ran, F. A., Cox, D., Lin, S., Barretto, R., Habib, N., Hsu, P. D., Wu, X., Jiang, W., Marraffini, L. A. et al. (2013). Multiplex genome engineering using CRISPR/Cas systems. *Science* **339**, 819-23.

Gao, J., Buckley, S. M., Cimmino, L., Guillamot, M., Strikoudis, A., Cang, Y., Goff, S. P. and Aifantis, I. (2015). The CUL4-DDB1 ubiquitin ligase complex controls adult and embryonic stem cell differentiation and homeostasis. *Elife* **4**.

Habibi, E., Brinkman, A. B., Arand, J., Kroeze, L. I., Kerstens, H. H., Matarese, F., Lepikhov, K., Gut, M., Brun-Heath, I., Hubner, N. C. et al. (2013). Whole-genome bisulfite sequencing of two distinct interconvertible DNA methylomes of mouse embryonic stem cells. *Cell Stem Cell* **13**, 360-9.

Hayashi, K., Ohta, H., Kurimoto, K., Aramaki, S. and Saitou, M. (2011). Reconstitution of the mouse germ cell specification pathway in culture by pluripotent stem cells. *Cell* **146**, 519-32.

Ho, L., Jothi, R., Ronan, J. L., Cui, K., Zhao, K. and Crabtree, G. R. (2009a). An embryonic stem cell chromatin remodeling complex, esBAF, is an essential component of the core pluripotency transcriptional network. *Proc Natl Acad Sci U S A* **106**, 5187-91.

Ho, L., Ronan, J. L., Wu, J., Staahl, B. T., Chen, L., Kuo, A., Lessard, J., Nesvizhskii, A. I., Ranish, J. and Crabtree, G. R. (2009b). An embryonic stem cell chromatin remodeling complex, esBAF, is essential for embryonic stem cell self-renewal and pluripotency. *Proc Natl Acad Sci U S A* **106**, 5181-6.

Kagiwada, S., Kurimoto, K., Hirota, T., Yamaji, M. and Saitou, M. (2013). Replication-coupled passive DNA demethylation for the erasure of genome imprints in mice. *EMBO J* **32**, 340-53.

Kawaguchi, M., Sugiyama, K., Matsubara, K., Lin, C. Y., Kuraku, S., Hashimoto, S., Suwa, Y., Yong, L. W., Takino, K., Higashida, S. et al. (2019). Co-option of the PRDM14-CBFA2T complex from motor neurons to pluripotent cells during vertebrate evolution. *Development* **146**.

Kim, T. W., Kang, B. H., Jang, H., Kwak, S., Shin, J., Kim, H., Lee, S. E., Lee, S. M., Lee, J. H., Kim, J. H. et al. (2015). Ctbp2 Modulates NuRD-Mediated Deacetylation of H3K27 and Facilitates PRC2-Mediated H3K27me3 in Active Embryonic Stem Cell Genes During Exit from Pluripotency. *Stem Cells* **33**, 2442-55.

Kurimoto, K., Yamaji, M., Seki, Y. and Saitou, M. (2008). Specification of the germ cell lineage in mice: a process orchestrated by the PR-domain proteins, Blimp1 and

Prdm14. *Cell Cycle* **7**, 3514-8.

Liang, J., Wan, M., Zhang, Y., Gu, P., Xin, H., Jung, S. Y., Qin, J., Wong, J., Cooney, A. J., Liu, D. et al. (2008). Nanog and Oct4 associate with unique transcriptional repression complexes in embryonic stem cells. *Nat Cell Biol* **10**, 731-9.

Ma, Z., Swigut, T., Valouev, A., Rada-Iglesias, A. and Wysocka, J. (2011). Sequence-specific regulator Prdm14 safeguards mouse ESCs from entering extraembryonic endoderm fates. *Nat Struct Mol Biol* **18**, 120-7.

Nady, N., Gupta, A., Ma, Z., Swigut, T., Koide, A., Koide, S. and Wysocka, J. (2015). ETO family protein Mtgr1 mediates Prdm14 functions in stem cell maintenance and primordial germ cell formation. *Elife* **4**, e10150.

Nakaki, F., Hayashi, K., Ohta, H., Kurimoto, K., Yabuta, Y. and Saitou, M. (2013). Induction of mouse germ-cell fate by transcription factors in vitro. *Nature* **501**, 222-6.

Niwa, H. (2014). The pluripotency transcription factor network at work in reprogramming. *Curr Opin Genet Dev* **28**, 25-31.

Ohno, R., Nakayama, M., Naruse, C., Okashita, N., Takano, O., Tachibana, M., Asano, M., Saitou, M. and Seki, Y. (2013). A replication-dependent passive mechanism modulates DNA demethylation in mouse primordial germ cells. *Development* **140**, 2892-903.

Okashita, N., Kumaki, Y., Ebi, K., Nishi, M., Okamoto, Y., Nakayama, M., Hashimoto, S., Nakamura, T., Sugasawa, K., Kojima, N. et al. (2014). PRDM14 promotes active DNA demethylation through the ten-eleven translocation (TET)-mediated base excision repair pathway in embryonic stem cells. *Development* **141**, 269-80.

Okashita, N., Sakashita, N., Ito, K., Mitsuya, A., Suwa, Y. and Seki, Y. (2015). PRDM14 maintains pluripotency of embryonic stem cells through TET-mediated active DNA demethylation. *Biochem Biophys Res Commun* **466**, 138-45.

Okashita, N., Suwa, Y., Nishimura, O., Sakashita, N., Kadota, M., Nagamatsu, G., Kawaguchi, M., Kashida, H., Nakajima, A., Tachibana, M. et al. (2016). PRDM14 Drives OCT3/4 Recruitment via Active Demethylation in the Transition from Primed to Naive Pluripotency. *Stem Cell Reports* **7**, 1072-1086.

Seki, Y. (2018). PRDM14 Is a Unique Epigenetic Regulator Stabilizing Transcriptional Networks for Pluripotency. *Front Cell Dev Biol* **6**, 12.

Seki, Y., Yamaji, M., Yabuta, Y., Sano, M., Shigeta, M., Matsui, Y., Saga, Y., Tachibana, M., Shinkai, Y. and Saitou, M. (2007). Cellular dynamics associated with the genome-wide epigenetic reprogramming in migrating primordial germ cells in mice. *Development* **134**, 2627-38.

Sim, Y. J., Kim, M. S., Nayfeh, A., Yun, Y. J., Kim, S. J., Park, K. T., Kim, C. H. and Kim, K. S. (2017). 2i Maintains a Naive Ground State in ESCs through Two Distinct Epigenetic Mechanisms. *Stem Cell Reports* **8**, 1312-1328.

Tu, S., Narendra, V., Yamaji, M., Vidal, S. E., Rojas, L. A., Wang, X., Kim, S. Y., Garcia, B. A., Tuschl, T., Stadtfeld, M. et al. (2016). Co-repressor CBFA2T2 regulates pluripotency and germline development. *Nature* **534**, 387-90.

Yamaji, M., Seki, Y., Kurimoto, K., Yabuta, Y., Yuasa, M., Shigeta, M., Yamanaka, K., Ohinata, Y. and Saitou, M. (2008). Critical function of Prdm14 for the establishment of the germ cell lineage in mice. *Nat Genet* **40**, 1016-22.

Yamaji, M., Ueda, J., Hayashi, K., Ohta, H., Yabuta, Y., Kurimoto, K., Nakato, R., Yamada, Y., Shirahige, K. and Saitou, M. (2013). PRDM14 ensures naive pluripotency through dual regulation of signaling and epigenetic pathways in mouse embryonic stem cells. *Cell Stem Cell* **12**, 368-82.

Yeo, J. C., Jiang, J., Tan, Z. Y., Yim, G. R., Ng, J. H., Goke, J., Kraus, P., Liang, H., Gonzales, K. A., Chong, H. C. et al. (2014). Klf2 is an essential factor that sustains ground state pluripotency. *Cell Stem Cell* **14**, 864-72.

Figures

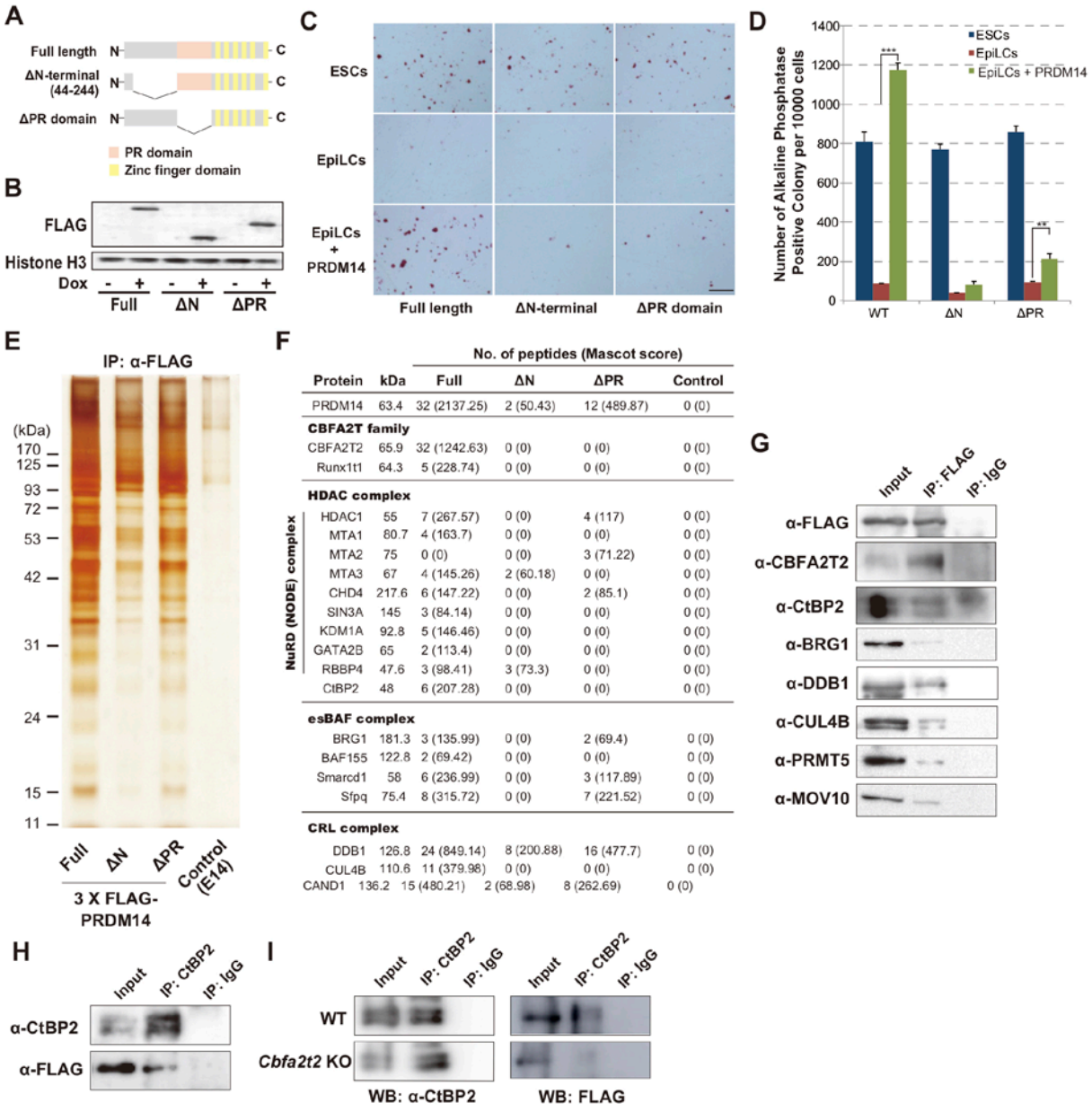

Figure 1. PRDM14 interacts with CtBP2 through CBFA2T2. (A) Scheme of full-length and deletion mutant of PRDM14. (B) The protein expression of full-length and deletion mutant of PRDM14 in ESCs with or without doxycycline. (C, D) Alkaline phosphatase staining of ESCs

and EpiLCs with or without exogenous *Prdm14* expression cultured in serum plus LIF for 3 days. Error bars indicate ± standard errors of the mean (SEM) of biological triplicates. *P* values were calculated by Tukey-Kramer multiple comparisons test. **P* < 0.05, ***P* < 0.01, ****P* < 0.001. (E) Silver staining of immunoprecipitants using whole cell extracts of full-length, *N*-terminal-, and PR domain deletion of PRDM14 in ESCs after *Prdm14* induction. (F) MS of peptide counts for full-length, *N*-terminal-, and PR domain deletion of PRDM14 in ESCs. (G) Immunoprecipitation with antibody against FLAG-PRDM14 using whole cell lysate of ESCs cultured in serum plus LIF after *Prdm14* induction followed by western blot with antibodies against indicated proteins. (H, I) Immunoprecipitation with anti-CtBP2 antibody using whole cell lysate of wild type (WT) or *Cbfa2t2* KO ESCs cultured in 2i plus LIF after *Prdm14* induction.

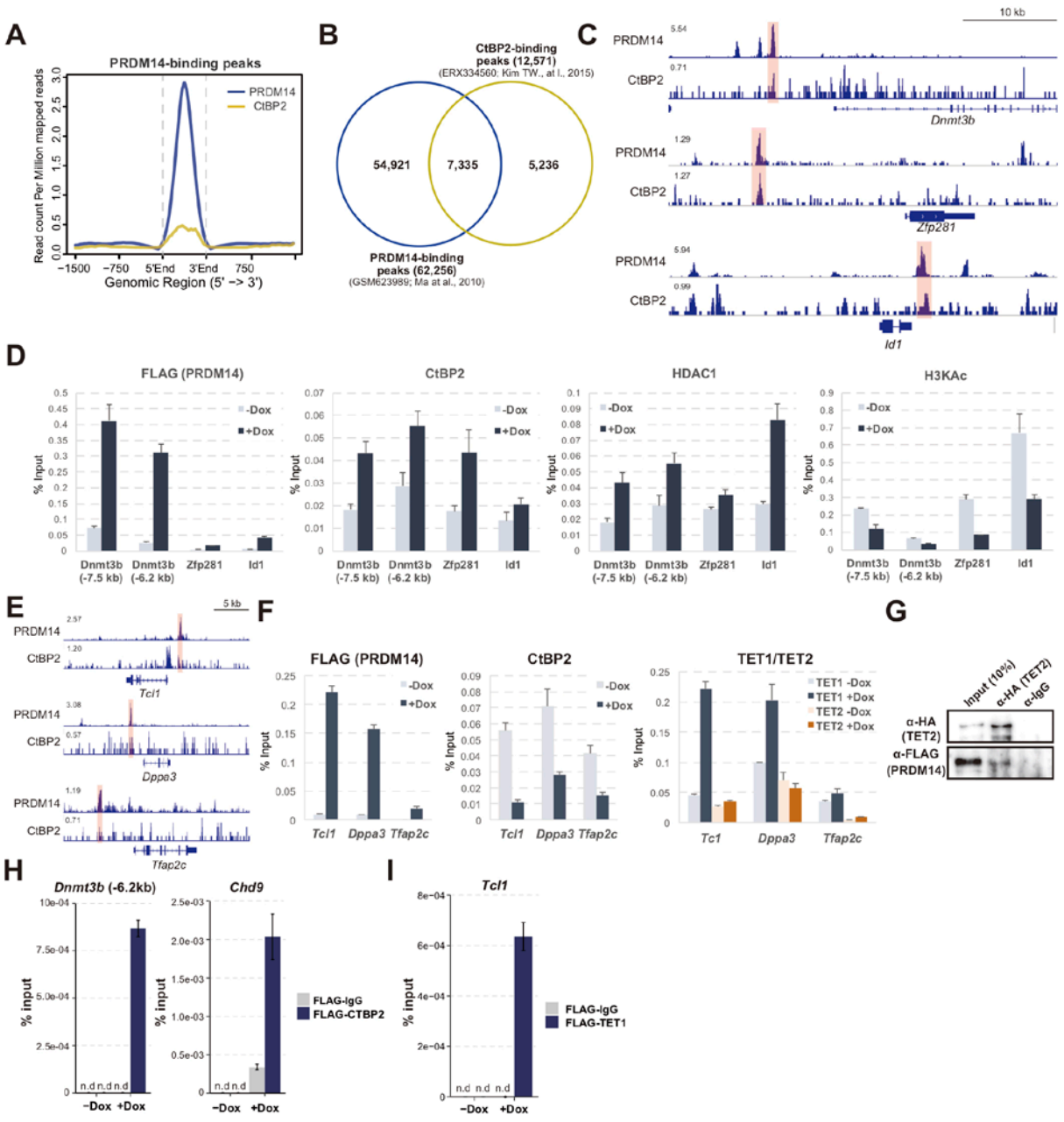

Figure 2. PRDM14 recruits CtBP2 at repressive but not active targets. (A) Histogram shows enrichment of PRDM14- and CtBP2-binding peaks near PRDM14-binding regions in ESCs. (B) Venn diagram shows overlapping PRDM14- and CtBP2-binding peaks. (C) Gene

tracks show that PRDM14-binding peaks colocalized with CtBP2 at repressive PRDM14 targets. (D) ChIP-qPCR of PRDM14, CtBP2, HDAC1, and H3KAc before and after *Prdm14* induction. Error bars indicate ± standard deviations of technical duplicates. (E) Gene tracks show that PRDM14-binding peaks did not colocalize with CtBP2 at active PRDM14 targets. (F) ChIP-qPCR of PRDM14, CtBP2, and TET1/TET2 before and after *Prdm14* induction at active PRDM14 targets. Error bars indicate ± standard deviations of technical duplicates. (G) Pull-down of recombinant HA-TET2 protein with recombinant FLAG-PRDM14 followed by western blotting with anti-HA or anti-FLAG antibodies. (H, I) Sequential ChIP (re-ChIP) was performed by initial immunoprecipitation with FLAG-antibody followed by CtBP2 (H) and (I) TET1 antibody, respectively. n.d. indicates non detection of qPCR amplification curves. Error bars indicate ± standard deviations of technical duplicates.

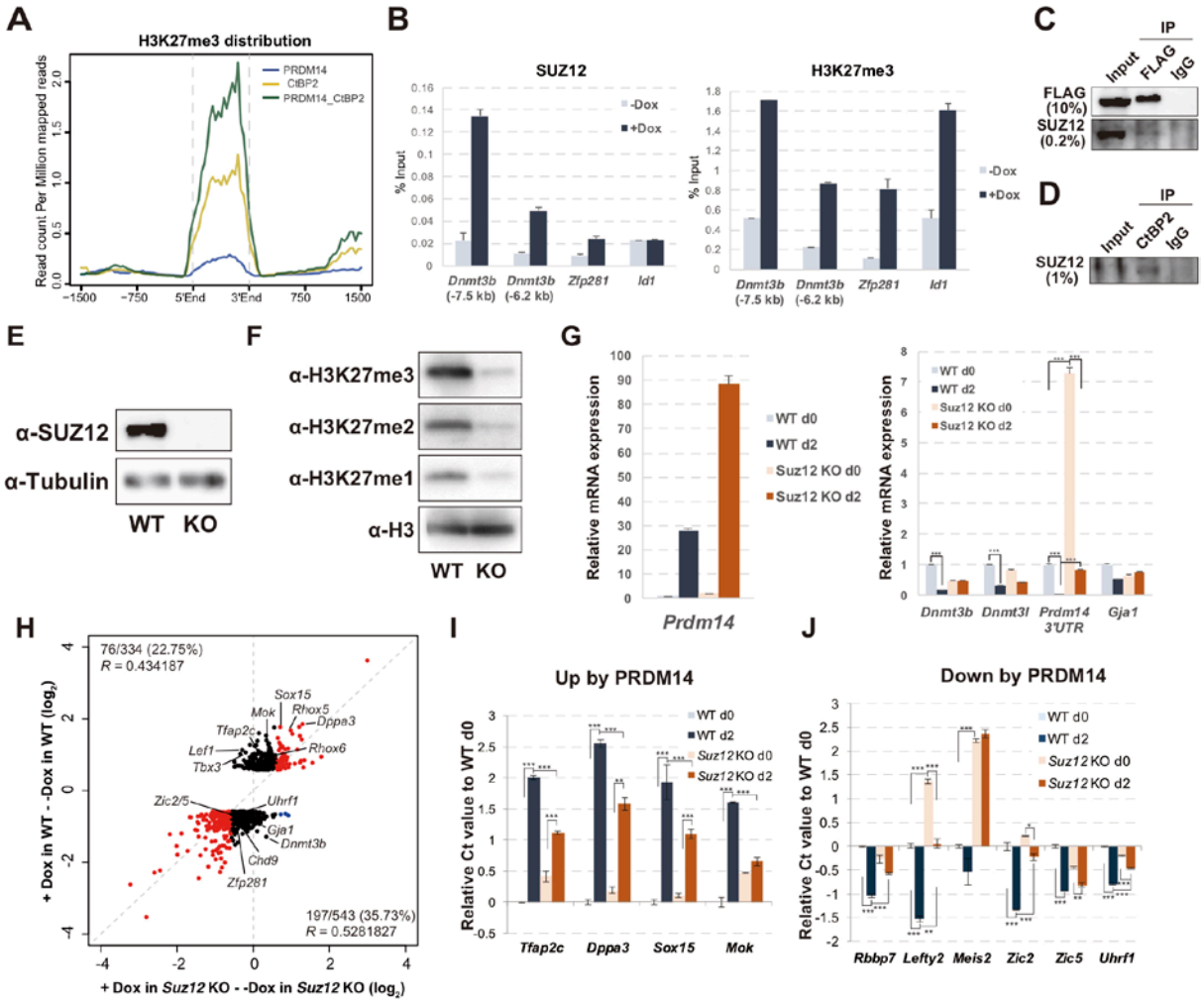

Figure 3. *Suz12* is partially involved in transcriptional PRDM14 repression in ESCs. (A) Histogram shows H3K27me3 enrichment near PRDM14- and CtBP2-binding peaks and PRDM14- and CtBP2-colocalized peaks in ESCs. (B) ChIP-qPCR of SUZ12 and H3K27me3 before and after *Prdm14* induction at repressive targets of PRDM14. Error bars indicate ± standard errors of the mean (SEM) of technical duplicates. (C, D) Immunoprecipitation using antibodies against FLAG or CtBP2 followed by western blot with indicated antibodies. (E, F)

Western blot with anti-SUZ12, tubulin, histone H3, and H3K27me1/2/3 antibodies in wild type (WT) and *Suz*12 KO ESCs. (G) qRT-PCR of indicated genes in wild type and *Suz12* KO ESCs before and after *Prdm14* induction. Error bars indicate ± standard errors of the mean (SEM) of biological triplicates. *P* values were calculated by Tukey-Kramer multiple comparisons test. **P* < 0.05, ***P* < 0.01, ****P* < 0.001. (H) Scatterplot of microarray data shows relative intensities of genes upregulated or downregulated by PRDM14 in wild type and *Suz12* KO ESCs. Red dots indicate genes upregulated and downregulated by PRDM14 in wild type and Suz12 KO ESCs. Blue dots indicate genes downregulated by PRDM14 in wild type ESCs and upregulated by PRDM14 in *Suz12* KO ESCs. *R* is correlation coefficient. (I, J) qRT-PCR of indicated genes in wild type and *Suz12* KO ESCs before and after *Prdm14* induction. Error bars indicate ± standard errors of the mean (SEM) of biological triplicates. *P* values were calculated by Tukey-Kramer multiple comparisons test. **P* < 0.05, ***P* < 0.01, ****P* < 0.001.

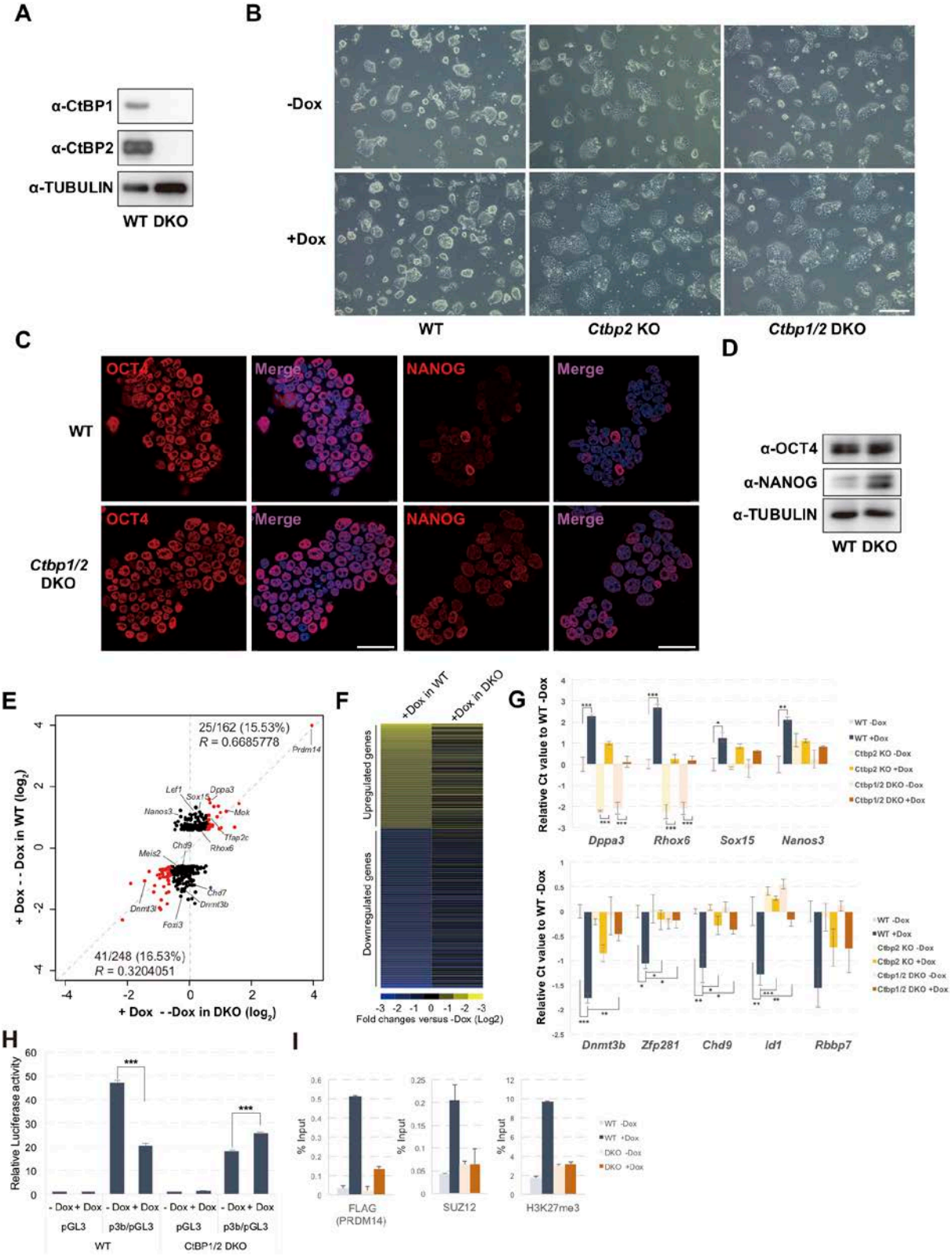

Figure 4. CtBP1/2 link PRDM14 to PRC2-mediated transcriptional repression. (A) Western blot of indicated protein in wild type (WT) and *Ctbp1/2* DKO ESCs. (B) Morphology of wild type, *CtBP2* KO, and *Ctbp1/2* DKO ESCs before and after *Prdm14* induction. Scale bar : 50 μ m (C) Immunofluorescence analysis of wild type and *Ctbp1/2* DKO ESCs with anti-OCT4 or NANOG antibody. Scale bar : 50 μm. (D) Western blotting of wild type and *Ctbp1/2* DKO ESCs with anti-OCT4, NANOG, and TUBLIN antibody. (E) Scatterplot of microarray data showing relative intensities of genes upregulated or downregulated by PRDM14 in wild type and *Ctbp1/2* DKO ESCs. Red dots indicate genes upregulated and downregulated by PRDM14 in wild type and *Ctbp1/2* KO ESCs. Blue dots indicate genes downregulated by PRDM14 in wild type ESCs and upregulated by PRDM14 in *Ctbp1/2* KO ESCs. *R* is correlation coefficient. (F) Heatmap shows relative expression levels of genes upregulated and downregulated by PRDM14 in wild type and Ctbp1/2 DKO ESCs. (G) qRT-PCR of indicated genes in wild type and *Ctbp1/2* DKO ESCs before and after *Prdm14* induction. Error bars indicate ± standard errors of the mean (SEM) of biological triplicates. *P* values were calculated by Tukey-Kramer multiple comparisons test. $*P < 0.05$, $**P < 0.01$, $***P < 0.001$. (H) Luciferase assay on *Dnmt3b* locus in wild type and *Ctbp1/2* DKO ESCs. Error bars indicate ± standard errors of the mean of biological triplicates. *P* values were calculated by Tukey-Kramer

multiple comparisons test. *$P < 0.05$, **$P < 0.01$, ***$P < 0.001$. (G) ChIP-qPCR analysis of PRDM14, SUZ12, and H3K27me3 in wild type and Ctbp1/2 DKO ESCs before and after *Prdm14* induction.

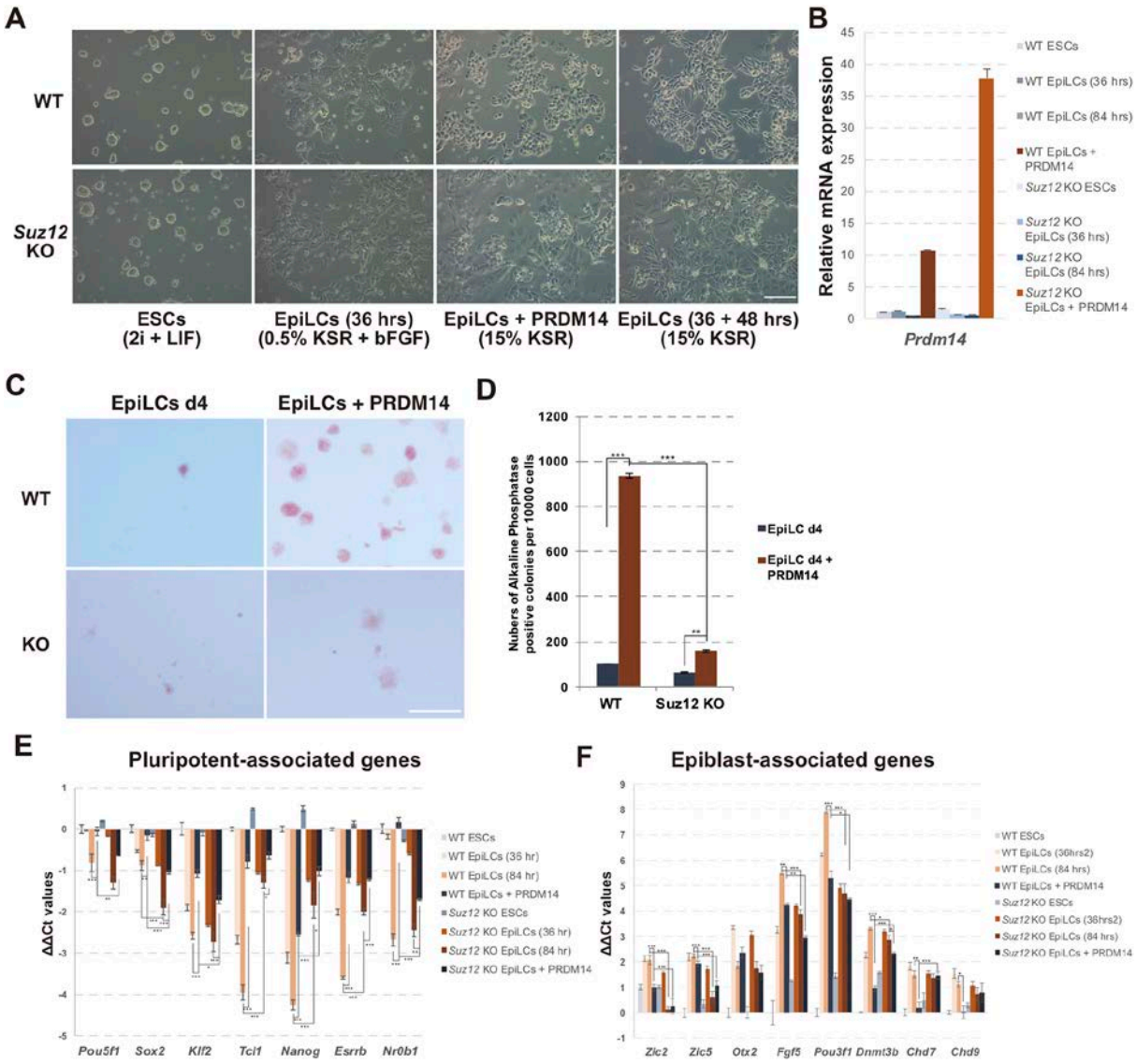

Figure 5. *Suz12* is required for PRDM14-mediated transition from primed to naïve pluripotency. (A) Morphology of wild type (WT), *Suz12* KO ESCs, and EpiLCs before and after *Prdm14* induction. (B) qRT-PCR of *Prdm14* in wild type and *Suz12* KO ESCs and EpiLCs before and after *Prdm14* induction. Error bars indicate ± standard errors of the mean of

biological triplicates. (C, D) Alkaline phosphatase staining of EpiLCs derived from wild type and *Suz12* KO ESCs before and after *Prdm14* induction. *P* values were calculated by Tukey-Kramer multiple comparisons test. **P* < 0.05, ***P* < 0.01, ****P* < 0.001. (E, F) qRT-PCR of indicated genes in wild type and *Suz12* KO ESCs, and EpiLCs before and after *Prdm14* induction. Error bars indicate ± standard errors of the mean of biological triplicates. *P* values were calculated by Tukey-Kramer multiple comparisons test. **P* < 0.05, ***P* < 0.01, ****P* < 0.001.

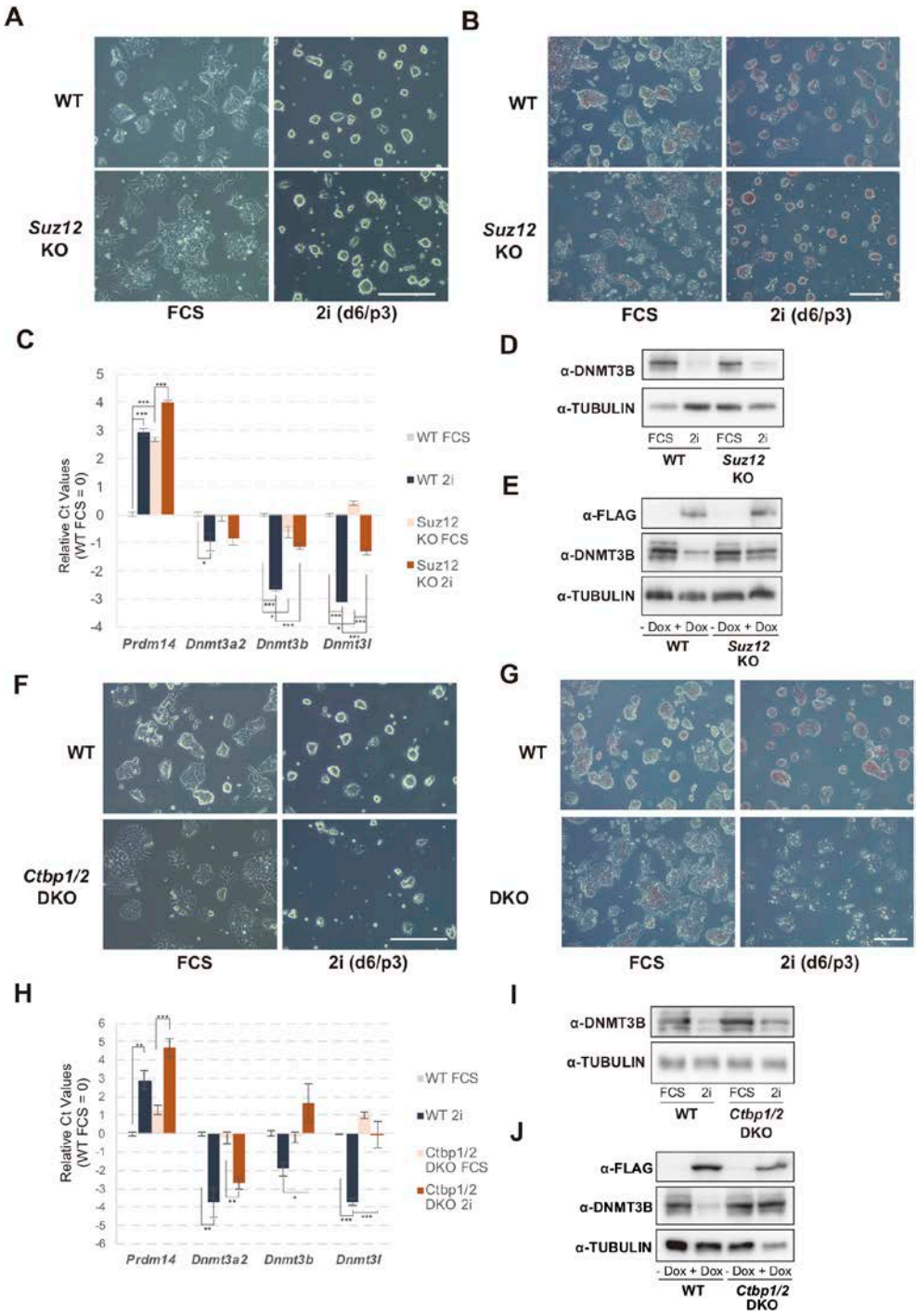

Figure 6. CtBP1/2-PRC2 axis is required for transcriptional *Dnmt3b/l* repression during transition from metastable- to ground-state pluripotency. (A) Morphology of wild type and

Suz12 KO ESCs in serum plus LIF or 2i plus LIF. Scale bar : 50 μm. (B) Alkaline phosphatase staining of wild type (WT) and *Suz12* KO ESCs under serum plus LIF or 2i plus LIF condition. Scale bar : 50 μ m. (C) qRT-PCR of indicated genes in wild type and *Suz12* KO ESCs in serum plus LIF or 2i plus LIF. Error bars indicate ± standard errors of the mean of biological triplicates. *P* values were calculated by Tukey-Kramer multiple comparisons test. **P* < 0.05, ***P* < 0.01, ****P* < 0.001. (D) Western blot of indicated proteins in wild type and *Suz12* KO ESCs in serum plus LIF or 2i plus LIF. (E) Western blot of indicated proteins in wild type and *Ctbp1* DKO ESCs before and after *Prdm14* induction. (F) Morphology of wild type and *Ctbp1/2* DKO ESCs in serum plus LIF or 2i plus LIF. Scale bar : 50 μm. (G) Alkaline phosphatase staining of wild type and *Ctbp1/2* DKO ESCs under serum plus LIF or 2i plus LIF condition. Scale bar : 50 μm. (H) qRT-PCR of indicated genes in wild type and *Ctbp1/2* DKO ESCs in serum plus LIF or 2i plus LIF. Error bars indicate ± standard errors of the mean of biological triplicates. *P* values were calculated by Tukey-Kramer multiple comparisons test. **P* < 0.05, ***P* < 0.01, ****P* < 0.001. (I) Western blot of indicated proteins in wild type and *Ctbp1/2* DKO ESCs in serum plus LIF or 2i plus LIF. (J) Western blot of indicated proteins in wild type and *Ctbp1/2* DKO ESCs before and after *Prdm14* induction.

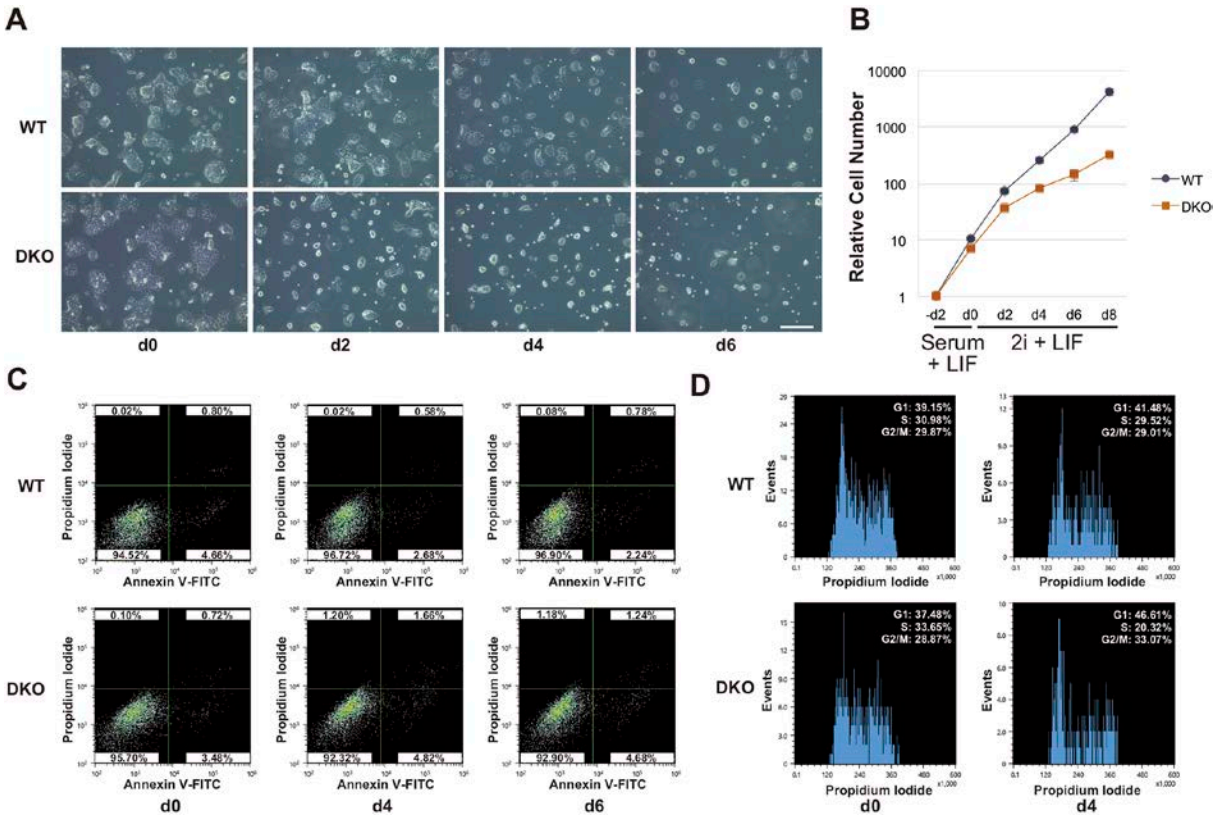

Figure 7. *Ctbp1/2* is required to maintain ground-state pluripotency. (A) Morphology of wild type (WT) and *Ctbp1/2* DKO ESCs during transition from metastable- to ground-state pluripotency. (B) Growth curves of wild type and *Ctbp1/2* DKO ESCs during transition from metastable- to ground-state pluripotency. (C) Apoptotic cells were monitored by propidium iodide and annexin V double staining. (D) Cell cycle distribution of wild type and *Ctbp1/2* DKO ESCs in serum plus LIF 4 d after transfer from serum plus LIF to 2i plus LIF.

Supplementary Figure 1

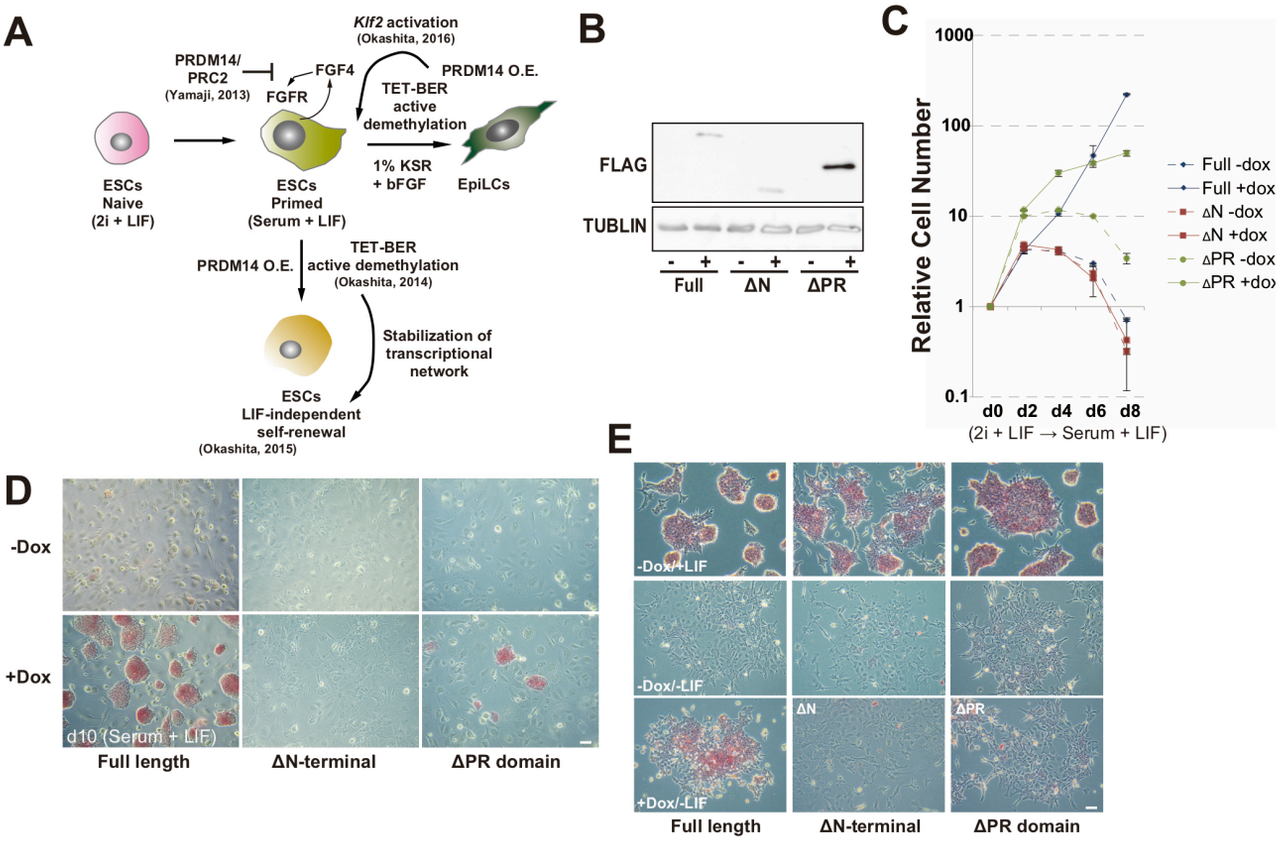

Supplementary Figure 1. (A) The scheme of the PRDM14 function in the maintenance and induction of pluripotency. (B) The establishment of *Prdm14*-inducible ESCs lacking endogenous *Prdm14*. (C) The proliferation rate of Prdm14-deficient ESCs with or without exogenous *Prdm14* in serum plus LIF condition. Error bars indicate ± standard errors of the mean (SEM) of biological triplicates.(D) Alkaline phosphatase staining of *Prdm14*-deficient ESCs with or without exogenous *Prdm14* ten days after the transfer to serum plus LIF condition. (E) Alkaline phosphatase staining of ESCs with or without exogenous *Prdm14* expression in serum plus LIF or serum minus LIF. Scale bar : 50 μm

Supplementary Figure 2

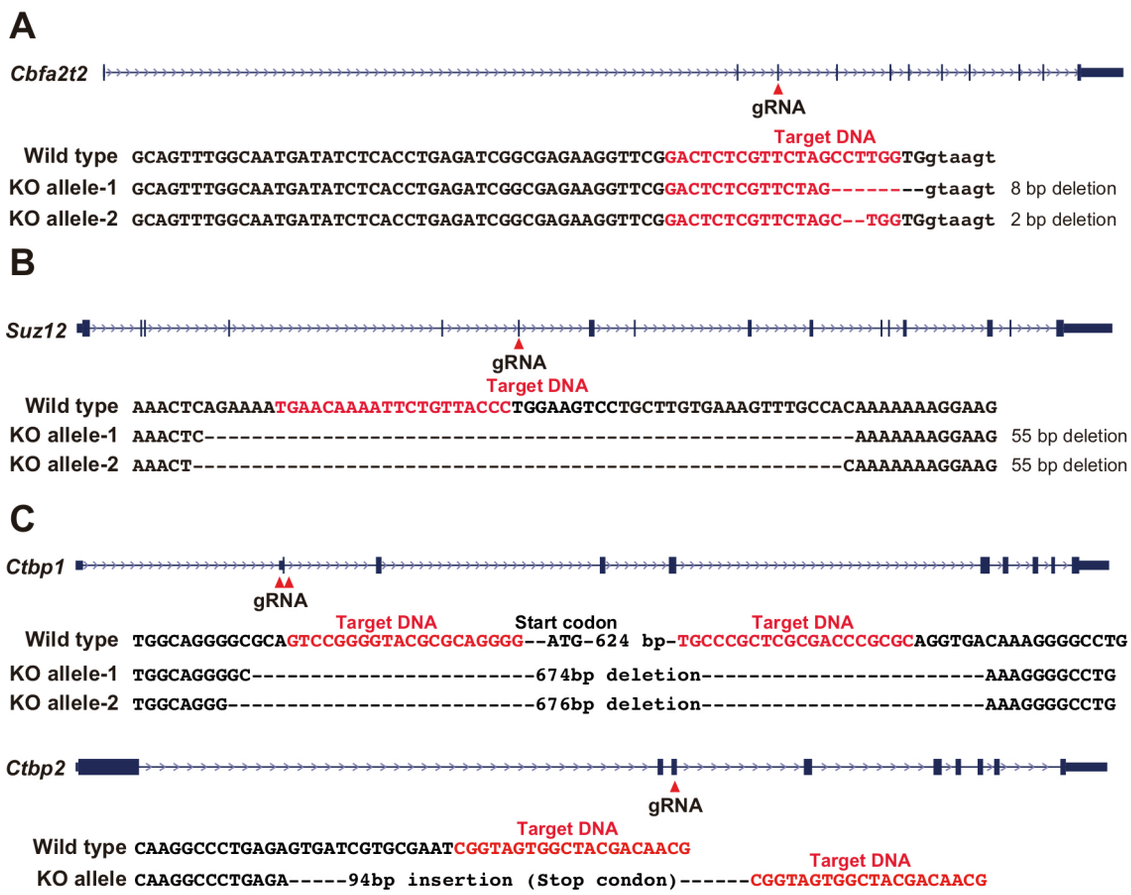

Supplementary Figure 2. The deletion sequence of *Cbfa2t2*, *Suz12* and *Ctbp1/2* locus by CRISPR/Cas9 system.

Table S1. Oligonucleotide lists for guide RNAs, qRT-PCR, HpaⅡ-qPCR and ChIP-qPC Guide RNA

Gene	Strand	Sequence(5'-3')
Ctbp1 upstream	Forward	CACCGTCCGGGGTACGCGCAGGGG
	Reverse	AAACCCCCTGCGCGTACCCCGGAC
Ctbp1 downstream	Forward	CACCGTGCCCGCTCGCGACCCGCGC
	Reverse	AAACGCGCGGGTCGCGAGCGGGCAC
Ctbp2	Forward	CACCGATCCGCCCCCAGCTGATGAA
	Reverse	AAACTTCATCAGCTGGGGGCGGATC
Cbfa2t2	Forward	CACCGACTCTCGTTCTAGCCTTGG
	Reverse	AAACCCAAGGCTAGAACGAGAGTC
Suz12	Forward	CACCGTGAACAAAATTCTGTTACCC
	Reverse	AAACGGGTAACAGAATTTTGTTCAC

ChIP-qPCR

Gene	Strand	Sequence(5'-3')
Dnmt3b (-7.5 kb)	Forward	GGGGGAATTACTTTGCCGGAG
	Reverse	TGCAATTCTCTATGGGGTCGC
Dnmt3b (-6.2 kb)	Forward	TCTTACCTCGGCTGGGAGAA
	Reverse	ACGAAGCTGAGAAGTTAGACCT
Zfp281	Forward	CATAGCCTGATGGAACCATTG
	Reverse	ATGTACGTTCTGCCCGTGAG
Id1	Forward	TGCAGATGGACCTGCTAAGTG
	Reverse	TCTCACACACAAACCCCTGTC
Tcl1	Forward	GCCCTGAGTGCAAACTTACAG
	Reverse	CTATGTGGTGTTGGGAAAAGC
Dppa3	Forward	CCTCGTGTGAGAATTTGCATC
	Reverse	GCCACGGCTATTCTATTCAGTG
Tfap2c	Forward	TCTAAAAAGCCCCTTGTGGAG
	Reverse	GACAGAGCCTCCCAGAGAAAG

qRT-PCR

Gene	Strand	Sequence(5'-3')
Prdm14 CDS	Forward	TGTGGTACGGAAATGGCTATG
	Reverse	AAACACCTTTCCACAGCGTTC
Prdm14 3'UTR	Forward	GGAATCCATTCAGACCAGGAG
	Reverse	GCACATAGTCGCTGGCTACAG
Dnmt3b	Forward	CTCGCAAGGTGTGGGCTTTTGTAAC
	Reverse	CTGGGCATCTGTCATCTTTGCACC
Dnmt3l	Forward	CCAGGGCAGATTTCTTCCTAAGGTC
	Reverse	TGAGCTGCACAGAGGCATCC
Gja1	Forward	GTGCAAGTGTGTAAGCGTGTG
	Reverse	CACAAAGATCCATGAGGAAGG

Tfap2c	Forward	ACGCGGAAGAGTATGTTGTTG
	Reverse	TTGTATGTTCGGCTCCAAGAC
Dppa3	Forward	AGGCTCGAAGGAAATGAGTTTG
	Reverse	TCCTAATTCTTCCCGATTTTCG
Sox15	Forward	TCCCCTTACCTATCCCCAGAC
	Reverse	AGTGTGCATTCTGGTTCCTTG
Mok	Forward	GGAGAAGACACCCATTATCAGAGA
	Reverse	GATATTCTCCGGCTTCACGTC
Rbbp7	Forward	GGGACCTGCGTAATCTGAAACT
	Reverse	GGCGATCAGTACCACTTGAGG
Lefty2	Forward	CAAAACACCGGGACTCTTAGG
	Reverse	TAAATGACATGGGCAAAGCTG
Meis2	Forward	AAGGCGCTTGCTCCTATCTC
	Reverse	TGGTTGTCAAAACACCATTCC
Zic2	Forward	AACTTCCCTAGCCCACTTTCC
	Reverse	TCCGGGAGTTTACAAATGGAC
Zic5	Forward	CTGAAGTCATGCGGACGATAC
	Reverse	CTAATTAGACCCGGTGGCAAG
Uhrf1	Forward	GCCACTTCTTCACTCCTCACC
	Reverse	CACATCTCAGCCTTCCATGAC
Rhox6	Forward	TTTCCAAGAGACTCGCTACCC
	Reverse	GTTCGCAGAACATCAGCACTC
Nanos3	Forward	AATCCTCTGCAGCTCCTGAAC
	Reverse	CACACATAATCCCGCAAAATG
Chd9	Forward	TAGATTGATTGGGGGAAGGTG
	Reverse	AAGTGGGACTGCATTGACTTG
Uhrf1	Forward	GCCACTTCTTCACTCCTCACC
	Reverse	CACATCTCAGCCTTCCATGAC
Id1	Forward	CAACAGAGCCTCACCCTCTC
	Reverse	AGAAATCCGAGAAGCACGAA
Pou5f1	Forward	CTCTCCCATGCATTCAAACTG
	Reverse	CCCCTGTTGTGCTTTTAATCC
Sox2	Forward	CTTGCTGGGTTTTGATTCTGC
	Reverse	AAGACCACGAAAACGGTCTTG
Klf2	Forward	CCCCAGGAAAGAAGACAGGAG
	Reverse	AGGCATTTCTCACAAGGCATC
Tcl1	Forward	GAACTTGCCTTCTTCCTCACG
	Reverse	TCACAGGTCAGGTGGGTACAG
Nanog	Forward	AGCCAGGTTCCTTCCTTCTTC
	Reverse	AAGATCTGACGCCCTCTTCTG
Esrrb	Forward	CGTGTGACAAGGAGACAGGAG
	Reverse	TCCAGCCACAACGTCATTATC
Nr0b1	Forward	GAAAGCGGTCGTAGCTGTAGG

	Reverse	GAAGCCAGTATGGAGCAGAGG
Otx2	Forward	GAGGTGATCCGGTGTTTTAGC
	Reverse	AATCAGTCGCACAATCCACAC
Fgf5	Forward	ATGAGTGCATCTGCTCTGCTC
	Reverse	CGTCTGTGGTTTCTGTTGAGG
Pou3f1	Forward	ATTTATTCGTGGAGCCTCTCG
	Reverse	TATACACAGATGCGGCTCTCG
Chd7	Forward	CGAGGAGAACCTGGACAAGAC
	Reverse	CTTTCAGTGGAACTGCTGCTG